

Immobilization laccase on heterophase TiO₂ microsphere as a photo-enzyme integrated catalyst for emerging contaminants degradation under visible light

Ying Zhang^{a,1}, Jing Gao^{a,1}, Xin Xin^a, Lihui Wang^a, Heyu Li^b, Xiaobing Zheng^{a,*}, Yanjun Jiang^{a,C,*}

^aSchool of Chemical Engineering and Technology, Hebei University of Technology, 8 Guangrong Road, Hongqiao District, Tianjin, 300130, China

^bTianjin UBasio Biotechnology Group Co., LTD., 276 Huanghai Road, TEDA, Tianjin, 300457, China

^cHebei Provincial Key Lab of Green Chemical Technology and High Efficient Energy Saving, Hebei University of Technology, 8 Guangrong Road, Hongqiao District, Tianjin 300130, China

ARTICLE INFO

Article history:

Received 9 July 2020

Revised 17 August 2020

Accepted 22 August 2020

Keywords:

Photo-enzyme integrated catalyst
TiO₂ heterostructure microsphere
Immobilized laccase
Visible light
Contaminants degradation

ABSTRACT

The successful combination of enzymes and photocatalysts in one pot is an elegant approach for the reactions with high efficiency. This combination usually requires both enzymes and photocatalysts with reasonable activity under the same condition. Herein, a photo-enzyme integrated catalyst by immobilizing laccase on clustered porous TiO₂ heterophase junction (HPJs) microsphere (denoted as mTiO₂-CVs) is synthesized for the first time. The TiO₂ microsphere with ordered regular radial structure and controllable heterophase junction (anatase/rutile) composition is prepared by a pressure-driven hydrothermal assembly method. The ratio of rutile and anatase phase of mTiO₂-CVs can be controlled by adjusting the amount of hydrochloric acid in the preparing process. The characterization results of mTiO₂-CVs prove that the mTiO₂-CVs has regular morphology, uniform mesoporous structure, larger specific surface area and narrower band gap, and can realize the effective utilization of visible light. After immobilizing laccase on mTiO₂-CVs by adsorption method, the integrated catalyst (mTiO₂-CVs2.5@lac) can be obtained. Compared with free laccase, mTiO₂-CVs2.5, and commercial P25, mTiO₂-CVs2.5@lac shows higher catalytic efficiency in the emerging contaminants degradation under visible light. Therefore, the photo-enzyme integrated catalyst presented in this study provides a promising platform for emerging organic pollutants degradation by combining the enzymes with photocatalysts

© 2020 Elsevier Ltd. All rights reserved.

1. Introduction

With the rapid development of modern industry, emerging organic contaminants (such as phenol, bisphenol A and triclosan, etc.) (EOCs) become an enormous threat to the balance of the ecosystem [1-3]. These EOCs can be migrated over a long distance via miscellaneous environmental media (atmosphere, water, organism, etc.) and exist in nature for a long time. Due to long-term residue, biological accumulation, semi-volatility and high-toxicity, they are seriously harmful to the environment and human health [4]. Thus, water pollution has been listed as a priority pollutant by many countries. Therefore, it is essential to develop efficient and

environmentally friendly technologies for the solution of EOCs remained in the environment.

Until now, a number of strategies such as photocatalytic degradation [5, 6], chemical oxidation [7], electrochemical oxidation [6, 8], and bio-degradation [9] have been reported to solute EOCs. Among these methods, semiconductor photocatalysis, an advanced oxidation process (AOP), is considered as an efficient green degradation technology [10]. Semiconductor photocatalyst can utilize the solar radiation as energy source to mineralize a variety of hazardous substances through generation of reactive oxygen species such as superoxide radical, which has a high oxidation or standard reduction potential [5, 11, 12]. Titanium dioxide (TiO₂) is one of the most promising photocatalysts for wastewater treatment because of its chemical durability, nontoxicity, environmental compatibility and functional diversity [13]. Nevertheless, the band gap width (~3.2 eV) of TiO₂ results in its insufficient solar energy consumption (only 4%) in degradation process [14]. Beyond that, the fast recombination of photogenerated electron-hole pairs further

* Corresponding authors.

E-mail addresses: zhengxiaobing@hebut.edu.cn (X. Zheng), yanjunjiang@hebut.edu.cn (Y. Jiang).

¹ Ying Zhang and Jing Gao contributed equally.

weaken the photogenerated redox reaction performances of TiO₂ [15]. For the sake of narrowing the band gap and suppressing the recombination of charge carriers, several strategies including cation or anion modification [16, 17], surface heterostructure construction [18] and defect introduction [19-21] have been developed. Although these methods can improve the photochemical performance of catalysts, the preparation process is usually complicated and other impurities are introduced. TiO₂ heterophase junction (HPJs) formed between different TiO₂ phases (anatase/brookite, rutile/brookite or anatase/rutile) without introducing new impurities, have been extensively investigated to promote the photocatalytic performance [13, 22-24]. Compared to single-phase TiO₂, TiO₂ HPJs can effectively narrow the band gap and then can utilize visible light. Meanwhile, the HPJs can promote charge separation and suppress photogenerated electron-hole pairs recombination. Nevertheless, it remains a big challenge to prepare TiO₂ with controllable HPJs through a simple process.

Bio-degradation is another efficient approach for organic contaminants degradation because of its high efficiency, safety and eco-friendliness, etc [25]. Laccase (EC 1.10.3.2), a multi-copper oxidase with relatively high redox potential, can degrade a variety of phenols to the comparative reactive quinones or form insoluble polymers by using molecular oxygen as oxidant [26]. However, there are some bottlenecks in the industrial application of free laccase such as high cost, difficulty in reuse and low stabilities [27]. Enzyme immobilization is considered as an ideal choice that could achieve reuse and improve the stabilities of free laccase. Up to now, various carriers are developed to immobilize laccase, such as porous glass [28], chitosan [29], silica nanoparticles [30], and nanoporous gold [31], etc. As a common inorganic material, TiO₂ has the characteristics of an ideal support for laccase immobilization, such as inexpensiveness, good biocompatibility and mechanical resistance [27]. On the basis of above properties, the construction of a novel TiO₂ material with large specific surface area and favorable structure matching well with enzyme molecules is of great significance for enzyme immobilization, as well as for the separation and reuse of the immobilized enzyme.

Although biocatalysis and photocatalysis are green, efficient and energy-saving methods for the degradation, their wide applications are blocked by the high cost and incomplete degradation. The combination of two or more catalytic approaches has been deemed an effective strategy to overcome these limits [32-34]. In previous reports, laccase was either directly fixed onto the original TiO₂ or directly mixed with TiO₂ powder for the degradation of pentachlorophenol or 2,4-DCP, but these attempts could only be performed under ultraviolet radiation and the enzyme would be rapidly deactivated under this condition [35]. To our knowledge, there is no report concerning the laccase immobilized on TiO₂ HPJs with excellent photocatalytic properties under visible light and its application in the synergistic complex pollutant degradation.

Thus, in this study, a photo-enzyme integrated catalyst by immobilizing laccase on clustered heterophase junction porous TiO₂ microsphere (denoted as mTiO₂-CVs) is synthesized for the first time. The obtained photo-enzyme integrated catalyst is used to realize the synergistic degradation of emerging organic contaminants under visible light. Specifically, the TiO₂ microsphere with ordered regular radial structure and controllable heterophase junction (anatase/rutile) composition is prepared by the pressure-driven hydrothermal assembly method. The controllable ratio of anatase phase and rutile phase is realized by adjusting the amount of HCl to boost the use of visible light and boost the photocatalytic capacity. Then, the TiO₂ microsphere is used for the efficient immobilization of laccase and finally applied to the synergistic 2,4-DCP degradation under visible light (>420 nm). Moreover, a possible mechanism of 2,4-DCP degradation by the photo-enzyme integrated catalyst is proposed. Commercial P25 is used as a reference

for photocatalytic properties and degradation effects. Moreover, emerging organic contaminants like 4-chlorophenol, bisphenol A, phenol and triclosan are selected for degradation tests to demonstrate the extensive degradation ability of the designed mTiO₂-CVs2.5 and mTiO₂-CVs2.5@lac.

2. Material and methods

2.1. Materials

Tetrabutyl titanate (TBOT) was purchased from Kermel. Pluronic F127 (PEO₁₀₆PPO₇₀PEO₁₀₆, Mw=12,600 g/mol) and laccase were purchased from Sigma-Aldrich. Glacial acetic acid (HOAc, 99.5%), concentrated HCl (36 wt%), 2,4-DCP, BPA and SA were purchased from Tianjin Kemiou Chemical Reagent. Tetrahydrofuran (THF, 99%) and 2,2-azinobis-3-ethylbenzothiazoline-6-sulfonic acid (ABTS) were purchased from Aladdin. Commercial P25 was purchased from Macklin.

2.2. Preparation of heterophase mTiO₂-CVs

The heterophase mTiO₂-CVs precursors were prepared by a typical solvent evaporation method [36]. Typically, 1.61 g of F127 and 2.0 mL of HOAc were added in 30 mL of THF solution. The pH of the reacting system was subsequently adjusted by changing HCl of amount ranged from 1.5 mL to 3.0 mL (the concentration of HCl is 4.3%, 5.7%, 7.1%, and 8.5%, respectively) and stirred for 10 min. 3.0 mL of TBOT and 0.2 mL H₂O were added dropwise subsequently for 10 min. The solution was kept in an oven at 45°C for 24 h.

The mTiO₂-CVs samples were prepared via a simple hydrothermal method. In a typical procedure, 1.5 g of the pale yellow gel were placed in a 50 mL Teflon-lined autoclave, and heated in an oven at 70°C for 24 h. The precipitates were washed three times by absolute ethyl alcohol and water, respectively, and then dried in an oven. Finally, the mTiO₂-CVs were obtained after being calcined successively under N₂ at 350°C for 3 h and in air at 400°C for 3 h in a tubular furnace.

2.3. Characterization

The morphology of mTiO₂-CVs was observed via scanning electron microscopy (SEM, FEI NanoSEM450 microscope under 5 KV accelerating voltages). The structures of mTiO₂-CVs were observed with a transmission electron microscope (TEM and HRTEM, JEOL-2100F under 4300V accelerating voltages). The elements of mTiO₂-CVs and mTiO₂-CVs@lac were investigated with energy dispersive X-ray spectrometry (EDS, FEI NanoSEM450 microscope under 5 KV accelerating voltages). X-ray powder diffractometer (XRD) on Bruker AXS D8 and Raman (Renishaw inVia Reflex Leica DM2700M microscope under 532 nm excitation wavelength) were used to detect the crystal structure of the mTiO₂-CVs. X-ray photoelectron spectroscopy (XPS, Thermo Scientific K-Alpha) was acquired to examine the element composition, chemical states and valance state of the mTiO₂-CVs samples. Confocal laser scanning microscopy (CLSM) was used to detect the distribution of laccase with a Leica TCS SP5 confocal microscope. The Fourier transform infrared (FT-IR) of the mTiO₂-CVs were performed with a Bruker, VECTOR22 spectrometer. Ultraviolet visible diffuse reflectance spectra (UV-DRS) were measured on a U-3010 spectrophotometer (Hitachi, Japan) UV-Vis spectrophotometer, using BaSO₄ as reference. The mTiO₂-CVs samples were also analyzed using electron paramagnetic resonance (EPR) spectroscopy (Brooke a300) and photoluminescence (PL) spectra (Fluorolog3-21 from Jobin Yvon. 243 nm was used as excitation wavelength, which shows good excitation at this excitation wavelength [37]). The BET surface area and BJH pore

size distribution were determined by Micromeritics ASAP 2020 system at 77 K.

2.4. Immobilized laccase on mTiO₂-CVs2.5 for preparing photo-enzyme integrated catalyst

2.4.1. Process of laccase immobilization

The immobilization of laccase on mTiO₂-CVs2.5 was operated as follows: 20 mg mTiO₂-CVs2.5 were added to 10 mL sodium citrate buffer (0.1 mol/L, pH=4.5) containing 2 mg of laccase. The mixture was placed in an incubator with 150 rpm at 25°C for shaking 15 min to reach adsorption equilibrium. The laccase immobilized on mTiO₂-CVs2.5 (mTiO₂-CVs2.5@lac) was separated by centrifugation (15000 rpm, 2 min). The mTiO₂-CVs2.5@lac was dried at -42°C in vacuum freeze, and the dry composite was placed at 4°C for the follow experiments.

2.4.2. Optimum condition of immobilized laccase

The effect of immobilization pH, temperature, time and initial laccase concentration on the properties of mTiO₂-CVs2.5@lac had been investigated. Typically, laccase solution (0.15 mg/mL-0.25 mg/mL) was mixed with mTiO₂-CVs2.5 (20 mg) in buffers with different pH (2.5-6.5) for certain time (5-50 min) at different temperature (15-45°C) with mild agitation. After that, the immobilized laccase was washed 3 times to remove the unabsorbed enzyme. The obtained immobilized laccase was kept at 4°C until further use.

2.4.3. Assay of the laccase activity

Generally, 0.1 mL free laccase (or 0.1 mL immobilized laccase) was added into 1.9 mL ABTS (1 mmol/L) and reacted at 25°C for 4 min. The activity of laccase was indicated by the increase of absorbance at the wavelength of 420 nm. One unit of activity (U) of laccase was defined as the amount of enzyme required to convert 1 μmol of ABTS to ABTS⁺ per minute in the test system.

2.5. Degradation of pollutant by the photo-enzyme integrated catalyst

2.5.1. Photo-enzyme integrated catalyst for contaminant degradation

The 2,4-DCP degradation catalyzed by photo-enzymatic catalysis (mTiO₂-CVs2.5@lac under light irradiation) and photocatalysis (mTiO₂-CVs2.5 under light irradiation) was carried out in a sodium citrate buffer at room temperature. A Xe lamp (300 W, Perfectlight Co., Ltd.) was used as the illumination source. Typically, 12 mg of the mTiO₂-CVs (or mTiO₂-CVs@lac) was dispersed in 20 mL 2,4-DCP (10 mg/L) solution with stirring. The solution was stirred for 0.5 h in the dark to reach adsorption equilibrium and turn on light. At given time intervals, 1.0 mL of samples was collected, centrifuged, and then analyzed at 285 nm by an UV-vis spectrophotometer. Similarly, enzymatic catalysis (mTiO₂-CVs2.5@lac under dark condition) was carried out under the same condition. The 2,4-DCP degradation rate was calculated as follows: degradation rate (%) = $(1-C/C_0) \times 100\%$, where C and C₀ are the concentrations of 2,4-DCP after and before reaction.

2.5.2. Evaluation of the reactive oxidizing species

Benzoquinone (BQ), tertiary butanol (TBA) and ethylene diamine tetracetic acid (EDTA) were used to eliminate •O₂⁻, •OH and h⁺ respectively for the scavenger collection experiments. 12 mg of the mTiO₂-CVs2.5 photocatalysts were added into 20 mL 2,4-DCP solution and stirred for 0.5 h in the dark. After that, the scavengers (1 mM) were added into the mixture and illuminated under Xe-lamp for 3.5 h with continuous stirring. Then, the suspension was collected, centrifuged, and analyzed at 285 nm by an UV-vis spectrophotometer.

2.5.3. Effect of different conditions on degradation

For investigating the effect of reaction conditions on the 2,4-DCP degradation catalyzed by mTiO₂-CVs2.5@lac (under light irradiation) and mTiO₂-CVs2.5 (under light irradiation), the effect of different pH values (2.5-8.5), catalysts concentration (0.2 mg/mL-1.5 mg/mL), reaction time (30-330 min) and initial 2,4-DCP concentration (10 mg/L-100 mg/L) was studied. The degradation rate of 2,4-DCP catalyzed by mTiO₂-CVs2.5 or mTiO₂-CVs2.5@lac was calculated at different reaction conditions. In addition, enzymatic catalysis (mTiO₂-CVs2.5@lac under dark condition) was carried out by the same method.

2.5.4. Reusability of the catalysts

Reusability of mTiO₂-CVs2.5 and mTiO₂-CVs2.5@lac were assessed under the optimized conditions. 12 mg of the mTiO₂-CVs2.5 or mTiO₂-CVs2.5@lac was added into 20 mL 2,4-DCP solution (10 mg/L) and stirred for 0.5 h in the dark. Then, the reactions were carried out under Xe-lamp irradiation, and then the mTiO₂-CVs2.5 and mTiO₂-CVs2.5@lac were separated at given time interval and washed with sodium citrate buffer. After that, the catalyst was added into a new reaction mixture for next reaction cycle.

2.5.5. The universal applicability of the photo-enzyme integrated catalyst

The 4-chlorophenol, bisphenol A, phenol and triclosan degradation catalyzed by P25, mTiO₂-CVs2.5@lac and mTiO₂-CVs2.5 under light irradiation were investigated in a sodium citrate buffer at room temperature. For comparison, laccase and mTiO₂-CVs2.5@lac catalyze the reactions under dark condition were also carried out. A Xe lamp (300 W, Perfectlight Co., Ltd.) was used as the illumination source. Typically, 12 mg of the catalysts were dispersed in 20 mL solution (10 mg/L) with stirring. The solution was stirred for 0.5 h in the dark to reach adsorption equilibrium and turn on light. At given time intervals, 1.0 mL of samples was collected, centrifuged, and then analyzed.

Reusability of mTiO₂-CVs2.5 and mTiO₂-CVs2.5@lac for degrading 4-chlorophenol, bisphenol A, phenol and triclosan were assessed. 12 mg of the mTiO₂-CVs2.5 or mTiO₂-CVs2.5@lac was added into 20 mL solution (10 mg/L) and stirred for 0.5 h in the dark. Then, the reactions were carried out under Xe-lamp irradiation. At given time intervals, mTiO₂-CVs2.5 and mTiO₂-CVs2.5@lac were separated and washed with sodium citrate buffer. After that, the catalysts were added into a new reaction mixture for next reaction cycle.

3. Results and discussion

3.1. Characterization of mTiO₂-CVs

The mTiO₂-CVs microspheres are prepared by a solvent-induced self-assembly evaporation method, and the fabrication procedures are schematically depicted in Fig. S1. The morphology and microstructure of the obtained mTiO₂-CVs samples are characterized by SEM, TEM and HRTEM. The SEM images (Fig. 1a-b) show that the mTiO₂-CVs are monodisperse cracked microspheres with obviously radial structure and the relative mean diameter is about 2.5 μm. TEM image (Fig. 1c) further reveals the cracked uniform spherical structures of the mTiO₂-CVs2.5 and 2.5 μm of the diameter, which is consistent with the result of SEM. The HRTEM image (Fig. 1d) recording from the surface of mTiO₂-CVs2.5 microsphere shows distinct lattice fringes with interplanar spaces of 0.233, 0.237 and 0.324 nm, which are well in accordance with the d₁₁₂ and d₀₀₄ plane of anatase and d₁₁₀ plane of rutile, respectively. There are abundant pores distributed on the surface of microspheres and in the radial structure. The corresponding EDS image of mTiO₂-CVs (Fig. 1e) reflects the existence of Ti and O, which

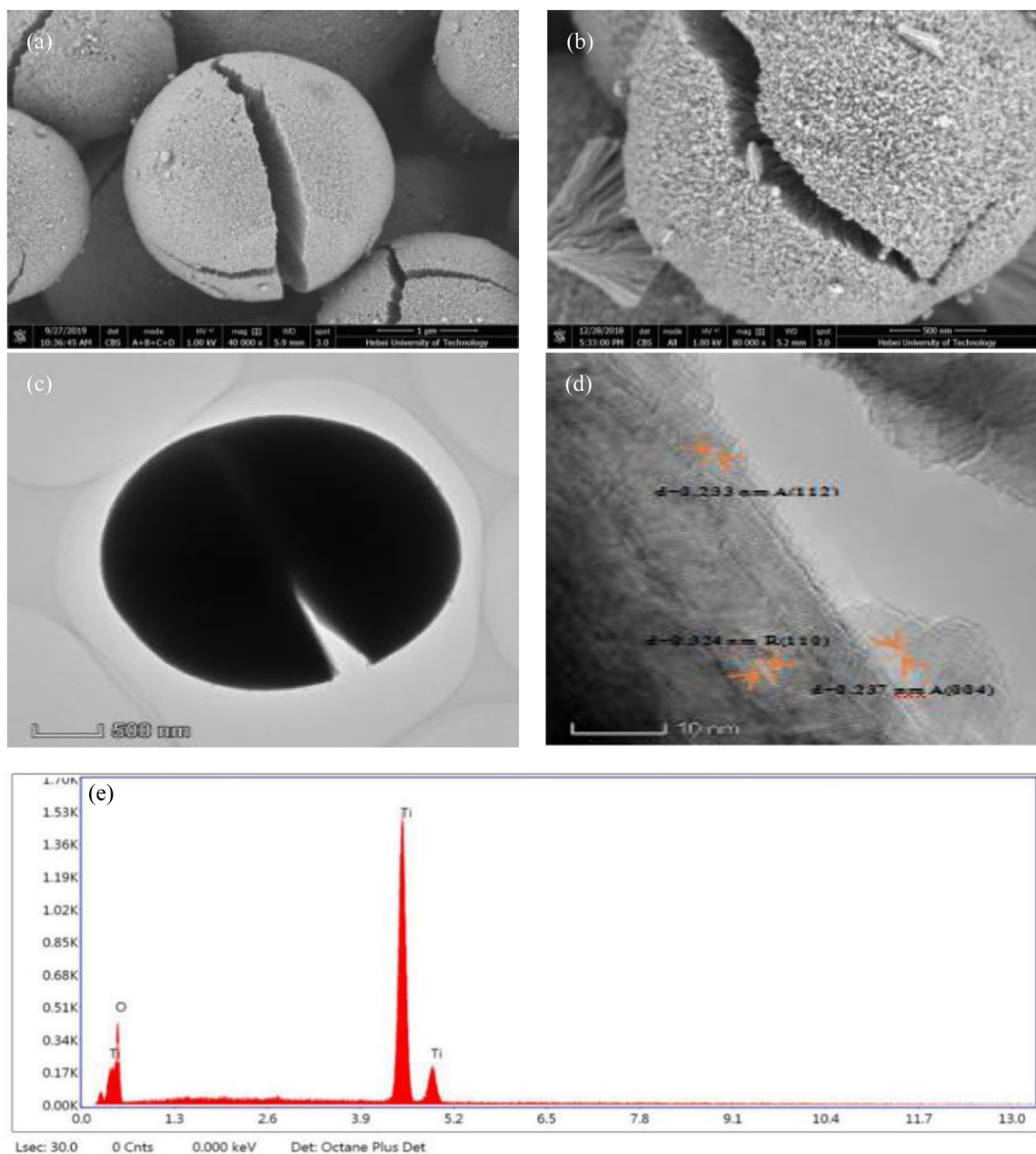


Fig. 1. SEM images of the $m\text{TiO}_2\text{-CVs}$ (a, b); TEM (c) and HRTEM (d) images of $m\text{TiO}_2\text{-CVs2.5}$ microsphere; the EDS image of $m\text{TiO}_2\text{-CVs2.5}$ (e).

proves the high purity of samples. Moreover, different amounts of HCl added during the preparation do not significantly change the sample morphology of $m\text{TiO}_2\text{-CVsX}$ (X represents the amount of HCl added during the synthesis process) as shown in Fig. S2. The element mapping of $m\text{TiO}_2\text{-CVs}$ (Fig. S3) indicates that Ti and O are evenly distributed in the microspheres. These results prove the fine crystallinity and mixed phase structure of $m\text{TiO}_2\text{-CVs}$ microspheres.

The formation process of TiO_2 HPJs is systematically investigated by XRD and Raman spectra. As revealed in Fig. 2a, when the added HCl amount is 1.5 mL, the XRD peaks of $m\text{TiO}_2\text{-CVs1.5}$ around 25.3° , 37.8° , 48.1° , 53.9° and 55.1° that are indexed to the 101, 004, 200, 105, 211 crystal facets of anatase phase (JCPDS No.21-1272) appear. As the amount of HCl increased, the peaks around 27.5° , 36.1° , 41.2° , 54.3° and 56.7° that indicate the characteristic intensity of rutile phase (JCPDS No.21-1276) appear and

grow gradually. At the same time, the strength of anatase phase characteristic peaks correspondingly decrease. When the amount of HCl is 2.0 or 2.5 mL, the characteristic peaks of rutile phase and anatase phase exist simultaneously and the ratio of A/R is 70.6:29.4 or 34.0:66.0, respectively. The A/R ratio of $m\text{TiO}_2\text{-CVs1.5}$ is very close to that of commercial P25 (86.4:13.6). When the HCl amount is 3.0 mL ($m\text{TiO}_2\text{-CVs3.0}$), only the representative peaks of rutile phase are discerned, while the peaks of anatase phase almost disappear. The above results indicate that the TiO_2 HPJs with different anatase/rutile phase ratios can be obtained by adjusting the amounts of HCl added in the synthetic process. The anatase/rutile ratios of $m\text{TiO}_2\text{-CVs}$ are summarized in Table S1. Fig. 2b shows Raman spectra (532 nm) of $m\text{TiO}_2\text{-CVs}$ and the commercial P25. There are six distinct well-defined peaks can be observed. The peaks at around 144, 395 and 516 cm^{-1} are representative the anatase phase vibrational modes [38]. Other peaks at 235, 445 and

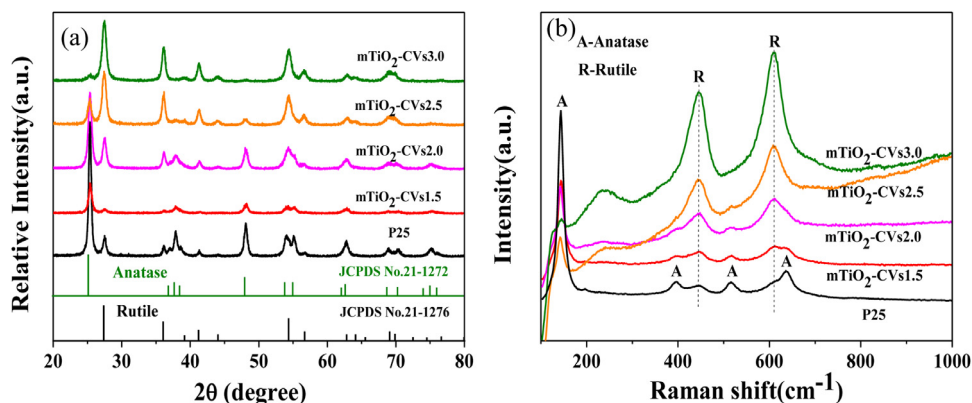


Fig. 2. XRD patterns (a) and Raman spectra (b) of mTiO₂-CVs.

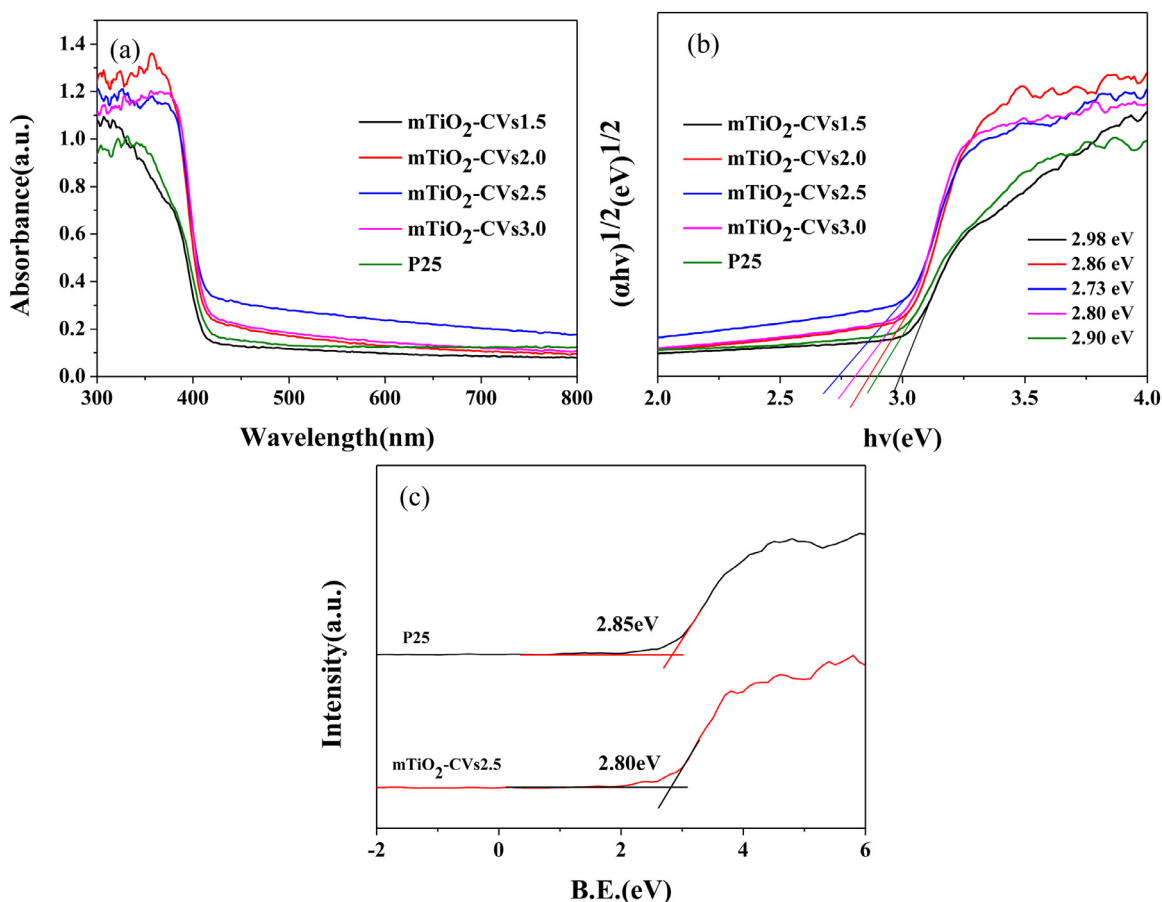


Fig. 3. (a) UV-vis diagram of different crystal phase ratios of mTiO₂-CVs; (b) the Kubelka-Munk function curve of mTiO₂-CVs; (c) XPS valence band spectrum of mTiO₂-CVs and P25.

608 cm⁻¹ are ascribed to the representative the rutile phase vibrational modes [37]. The simultaneous existence of two characteristic peaks in mTiO₂-CVs further demonstrates the successful preparation of heterophase junction, which is consistent with the results of HRTEM. These results confirm that HCl is beneficial for the growth of rutile and formation of HPJs.

The visible-light absorbance properties of all samples are measured with UV-vis DRS (Fig. 3). It is clear that the absorption range of mTiO₂-CVs1.5 is close to that of P25. Compared to P25, the absorption range of mTiO₂-CVs2.0, mTiO₂-CVs2.5 and mTiO₂-

CVs3.0 occur obvious red shift. The absorption edges of mTiO₂-CVs1.5, mTiO₂-CVs2.0, mTiO₂-CVs2.5, mTiO₂-CVs3.0 and P25 appear around 413, 436, 457, 448 and 417 nm, respectively. The band gap energies of P25, mTiO₂-CVs1.5, mTiO₂-CVs2.0, mTiO₂-CVs2.5 and mTiO₂-CVs3.0 are estimated to be 2.89, 2.98, 2.86, 2.73 and 2.80 eV by Kubelka-Munk transformation, respectively (Fig. 3b). Among, the band gap value of P25 is the same as that reported in the previous study [37]. The valence band for P25 and mTiO₂-CVs2.5 are calculated to be at 2.85 and 2.80 eV respectively by using VB XPS curves (Fig. 3c). The heterophase junction prepared by

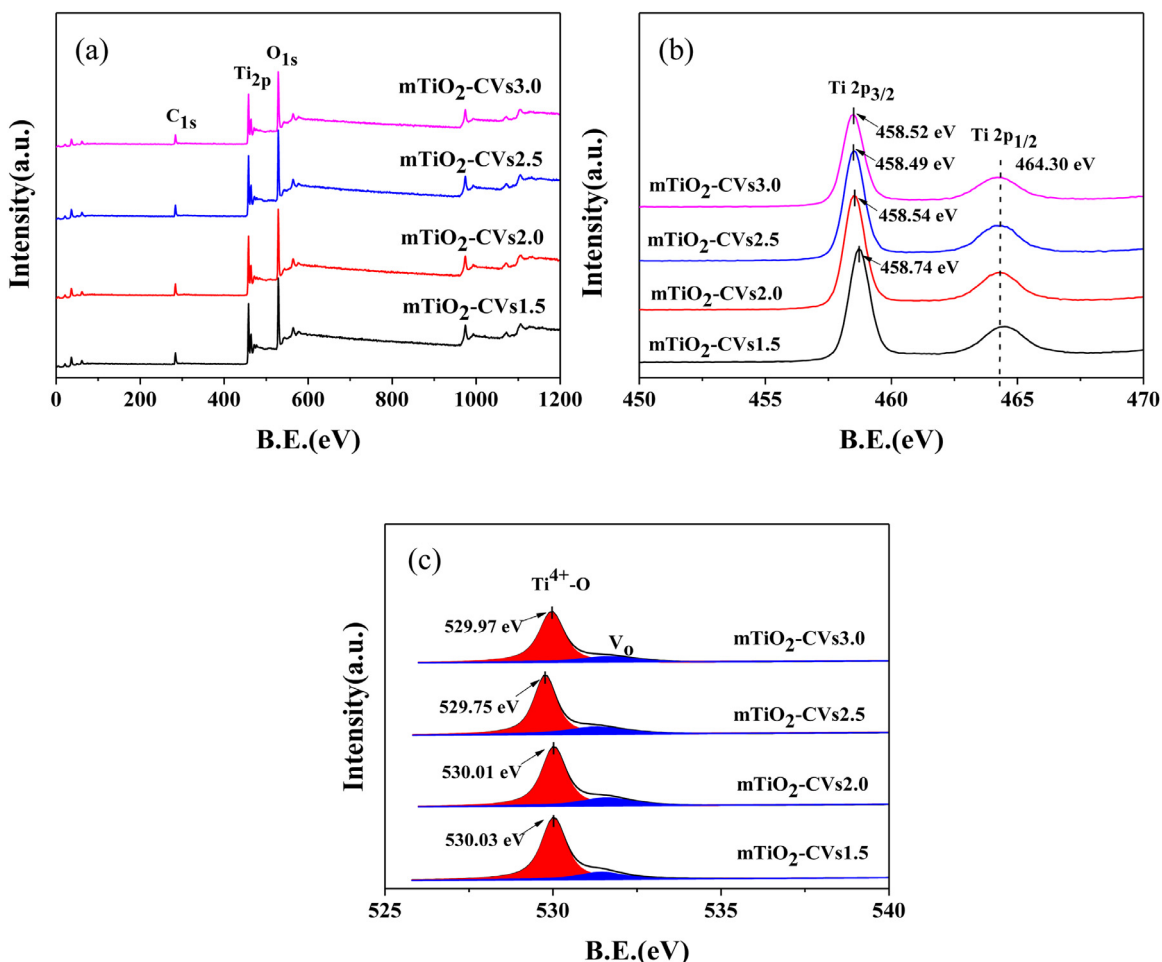


Fig. 4. XPS spectra of mTiO₂-CVs: (a) survey spectra, (b) high-resolution spectra of Ti 2p, (c) high-resolution spectra of O 1s.

adjusting the amount of HCl not only broadens the light edge of mTiO₂-CVs from ultraviolet region to the visible region, but also narrows the band and valence gap. The larger absorption range of mTiO₂-CVs conduce to the utilization of visible light. Moreover, the lower band gap energy can accelerate the formation of photogenerated electron-hole pairs and improve photocatalytic efficiency.

The element composition and chemical state of mTiO₂-CVs are investigated by XPS. The full XPS survey (Fig. 4a) indicates that all the samples exhibit obvious similar binding energy (BE) peaks and are primarily composed of Ti, O and C elements. In the high resolution Ti 2p spectrum of mTiO₂-CVs (Fig. 4b), the two peaks at binding energies of 458.5 and 464.3 eV can attribute to Ti 2p_{3/2} and Ti 2p_{1/2} of Ti⁴⁺ chemical states in the TiO₂ lattice, respectively. Compared to mTiO₂-CVs1.5, the curves of other three samples slightly shift to lower binding energy, which is ascribed to the introduction of oxygen vacancies (V_O) [39]. O 1s spectrum of mTiO₂-CVs can be divided into a main peak at 529.8 eV and a absorption shoulder at 531.0 eV (Fig. 4c), which are attributed to the lattice oxygen in TiO₂ (Ti⁴⁺-O) and the surface V_O, respectively [40, 41]. The Ti⁴⁺-O peak has shifted by 0.02 eV, 0.28 eV and 0.06 eV from mTiO₂-CVs1.5 to mTiO₂-CVs2.0, mTiO₂-CVs2.5 and mTiO₂-CVs3.0 respectively, which is induced by the surplus electrons from the oxygen defects in the mTiO₂-CVs crystal lattice [40]. Meanwhile, in the light of the peak area ratios, the concentrations of surface V_O in mTiO₂-CVs1.5, mTiO₂-CVs2.0, mTiO₂-CVs2.5 and mTiO₂-CVs3.0 are estimated to be 18.5%, 24.5%, 26.0% and 22.8%, respectively [39]. In a high amount of HCl, oxygen atom from lattice site can be ab-

stracted by hydrogen atom to form H₂O molecule and then escape from the surface of mTiO₂-CVs to eventually form V_O on the surface. The O₂ molecule can be adsorbed by V_O and split into oxygen atoms, which can diffuse into the crystal of mTiO₂-CVs and eventually form a lot of superoxide radicals for redox reactions [41]. In contrast, excess HCl in the preparation process can break the phase connection, resulting in the decrease of V_O concentration [39]. Therefore, the V_O can be controllably introduced by changing the HCl amount and then the photo-catalytic performance can be improved.

In order to further reveal the charge separation property of the mTiO₂-CVs, various behaviors of native defects such as oxygen vacancies are confirmed by EPR spectroscopy (Fig. 5). The spectra of mTiO₂-CVs exhibits a strong signal at g=2.007 ranging from 1.93 to 1.99, which could be mainly induced by the presence of V_O [42]. Beyond that, the EPR intensity of V_O enhances with the increase of HCl amount until 2.5 mL and then decreases when the amount of HCl is 3.0 mL. These results indicate that the addition of appropriate strong acids can cause an oxygen-deficient environment leading to the extra formation of V_O. V_O can actually enact electron capture traps that simultaneously boost the charge separation and inhibit the recombination rate of charge carriers [43]. However, excess HCl may destroy the phase junction in mTiO₂-CVs, and simultaneously generate some unwanted recombination centers, resulting in a significant decrease of electron-hole pairs separation efficiency [39, 44]. The transition of electrons from valence band maximum (VBM) to V_O level and from V_O to CBM can cause

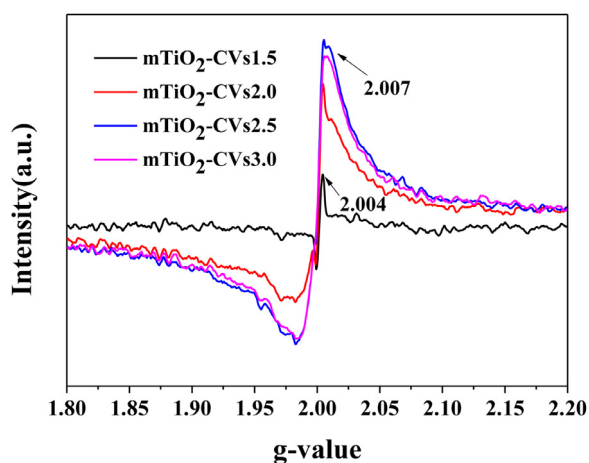


Fig. 5. EPR spectra of mTiO₂-CVs.

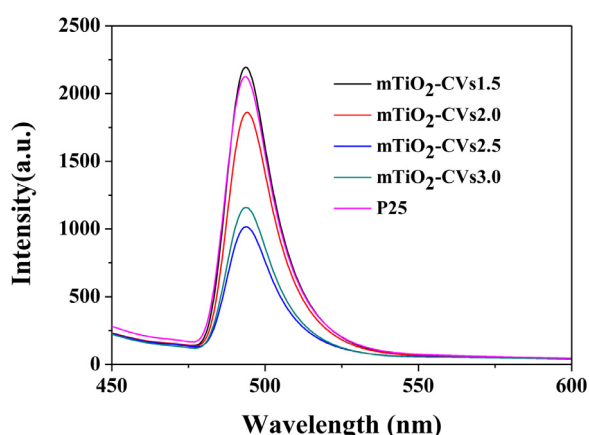


Fig. 6. The fluorescence spectroscopy of mTiO₂-CVs and P25.

visible light absorption. Hence, the appropriate formation of surface V_0 introduced by regulating the amount of HCl can promote the charge separation and improve the photocatalytic activity.

The photoluminescence (PL) spectra is employed to study the charge separation property of photogenerated electron-holes in the as-prepared mTiO₂-CVs. Fig. 6 shows the PL emission spectra of mTiO₂-CVs and P25 at 243 nm excitation wavelength. The emission peak centered at 494 nm is attributed to the recombination of the photoelectron hole pairs [22]. Meanwhile, with the increase of the added HCl amount during the reaction, the ratio of rutile in the crystal phase proportion increases gradually and the intensity of mTiO₂-CVs shows an obvious trend of decreasing first and then increasing. As a result, the mTiO₂-CVs2.5 exhibits the lowest luminous intensity, indicating that the HPJs introduced by appropriate amount of HCl has excellent charge separation property and can efficiently suppress the charge recombination.

The BET surface area and the BJH pore size distributions of the mTiO₂-CVs are also analyzed by N₂ adsorption-desorption isotherms. As can be seen from Fig. 7a, with the amount of HCl increases from 1.5 mL to 3.0 mL, all the isotherms of mTiO₂-CVs and P25 show characteristic type IV isotherms with a H3-type hysteresis loop. These results suggest that the mTiO₂-CVs have loose slit-like pores and ordered mesoporous network structure resulting from the aggregation of TiO₂ nanoparticles [45]. Furthermore, the pore size distribution is estimated by the BJH model (Fig. 7b). The specific surface area and pore volume values of mTiO₂-CVs and commercial P25 are summarized in Table S1. The pore sizes of mTiO₂-CVs and P25 are centered at around 7.11 nm and 3.9

nm, respectively. Compared with commercial P25, mTiO₂-CVs exhibit larger pore volume and specific surface area. Especially, the mTiO₂-CVs2.5 has the largest surface area (93.34 cm²/g). The favorable specific surface area and internal pore structure are beneficial to the multiple reflection and refraction of light, thus boosting the utilization efficiency of light and raising the photocatalytic ability. On the other side, the unique internal structure of mTiO₂-CVs provides abundant active sites for reactions and enzyme immobilization.

3.2. Growth mechanism of mTiO₂-CVs heterophase junction

During the preparation of mTiO₂-CVs, the added amount of HCl can affect the hydrolysis and condensation of TBOT, leading to the growth of different crystalline phases of anatase and rutile. As shown in Fig. S4, in the condensation process, the coordination of Ti⁴⁺ ions with the OH⁻ and Cl⁻ ions plays a crucial role in the formation of crystal phase and HPJs, thus [Ti(OH)_nCl_m]²⁻ (n+m=6) octahedra are formatted by inducing partially hydrolyzed, where n and m represent the acidity and the concentration of Cl⁻, respectively. The nucleation and growth processes of anatase and rutile proceed via the dehydration and cross-linking between [Ti(OH)_nCl_m]²⁻ octahedra [46]. At low amount of HCl, high OH⁻ concentration and low Cl⁻ concentration increase the hydrolysis of TBOT, which is conducive to the formation of anatase phase. On the contrary, large amounts of HCl greatly reduce the OH⁻ in the solution and high concentration of Cl⁻ inhibits the hydrolysis and condensation of TBOT, which is conducive to the nucleation and growth of rutile [47]. In addition, rutile phase preferentially forms V_0 because the Ti-O bond is longer in octahedral structural units than in anatase [48]. Different ratios of anatase and rutile between HPJs generate varied interfacial contact areas, which will cause diverse surface bands bending at the space charge region in the built-in electric field. The ratio optimization of HPJs is also an optimization process of the built-in electric field for space charge separation in the anatase/rutile phase junction region [49]. By this simple method, the TiO₂ heterophase junction with different anatase/rutile phase ratios can be introduced. In addition, the difference phase ratios further affect the photocatalytic activities of mTiO₂-CVs.

3.2.1. Degradation of 2,4-DCP by mTiO₂-CVs

The photocatalytic activity of mTiO₂-CVs is assessed via the 2,4-DCP degradation with different time under visible light in order to compare the degradation effects of different catalysts (>420 nm). Commercial P25 is used as a comparative catalyst, and blank experiment is conducted simultaneously. As shown in Fig. 8, according to the results of the blank test, the self-photolysis of 2,4-DCP can be neglected. The degradation rate of 2,4-DCP catalyzed by mTiO₂-CVs1.5, mTiO₂-CVs2.0, mTiO₂-CVs2.5, mTiO₂-CVs3.0 and P25 is 37.7%, 53.9%, 59.1%, 50.1% and 46.8% respectively after 3.5 h reaction under visible light. Most of mTiO₂-CVs except mTiO₂-CVs1.5 show better degradation rate than that of P25, among which mTiO₂-CVs2.5 (A/R is 34.0:66.0) is the best. This result is consistent with the literature reports [50, 51]. By regulating the amount of HCl to adjust the anatase/rutile ratio of HPJs in mTiO₂-CVs, the light utilization of this photocatalyst extends from ultraviolet to visible light. What's more, the mTiO₂-CVs achieve or even exceed commercial P25 in photocatalytic 2,4-DCP degradation. These results imply that the introduced HPJs plays a vital role in photocatalyst preparation and the 2,4-DCP degradation. Nonetheless, a higher rutile percentage in HPJs such as mTiO₂-CVs3.0 can result in a decrease of 2,4-DCP degradation. This decrease may be caused by extra high concentration of HCl, leading to the destruction of the phase interface as well as weakening the separation and photoelectron hole pairs transfer efficiency. The EPR

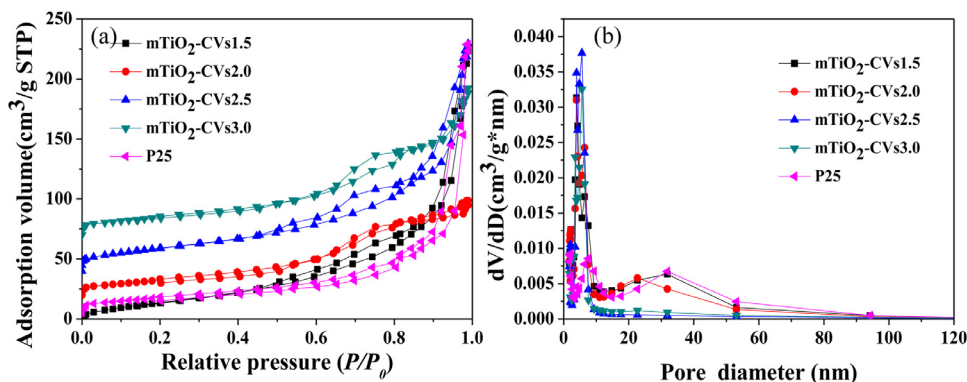


Fig. 7. (a) N_2 adsorption-desorption isotherms and (b) the corresponding pore size distribution curves of the $mTiO_2$ -CVs and P25.

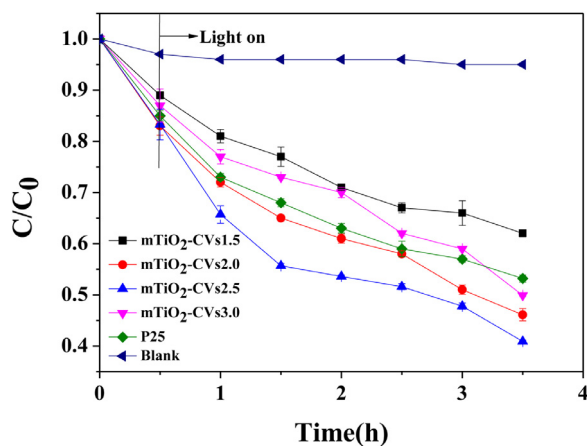


Fig. 8. The photocatalytic 2,4-DCP (10 mg/L; pH=5.5) of the different photocatalysts under visible light.

results also confirm these results. In the $mTiO_2$ -CVs2.5, the successful construction of the HPJs and the appropriate A/R phase ratio not only reduce the band gap and realize the utilization of visible light, but also promote the excitation of photogenic electron-hole pairs, and improve the separation and transport of charge. In addition, the relative high specific surface area and unique aperture structure realize multiple reflection of light and provide more reactive sites. Thus, $mTiO_2$ -CVs2.5 is selected as photo-catalyst in the subsequent experiments.

3.2.2. Evaluation of the reactive oxidizing species

Usually, it is ascertained that the removal of pollutants by photocatalysis is related to several reactive oxygen species (ROS) including photo-generated holes (h^+), superoxide radical ($\bullet O_2^-$) and hydroxyl radical ($\bullet OH$) [11]. In order to verify the main ROS of 2,4-DCP degradation, the radicals trapping experiments are implemented with the addition different scavenger agents. Benzoquinone (BQ), ethylene diamine tetracetic acid (EDTA) and tertiary butanol (TBA) are adopted to quench $\bullet O_2^-$, h^+ and $\bullet OH$, respectively. Typically, $mTiO_2$ -CVs2.5 is added into the 2,4-DCP mixture and stirred for 0.5 h in the dark. After that, the scavengers (1 mM) are added into the liquor and irradiated under visible light for 3.5 h with continuous stirring. From Fig. 9, the 2,4-DCP degradation is strongly inhibited in the existence of BQ, but it is slightly affected by TBA and EDTA. This means that 2,4-DCP was oxidized and decomposed mainly via the $\bullet O_2^-$ as the active intermediate.

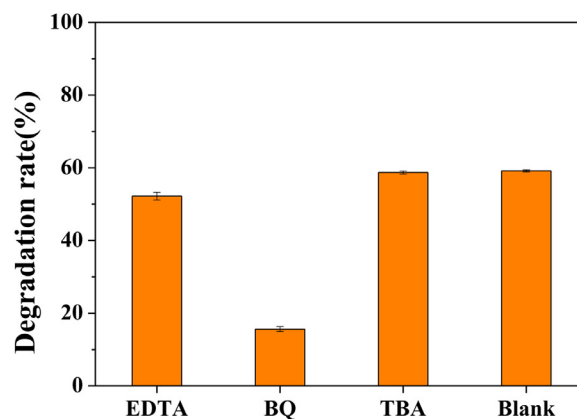


Fig. 9. Scavenger trapping experiments of $mTiO_2$ -CVs2.5.

3.3. Preparation of photo-enzyme integrated catalyst

Based on the above results, the obtained $mTiO_2$ -CVs can not only realize the efficient utilization of visible light, but also boost the degradation rate of 2,4-DCP compared with the commercial P25. Nevertheless, the degradation rate is still not satisfactory. In the following research, the $mTiO_2$ -CVs2.5 are used for the immobilization of laccase, a widely used enzyme in degradation of CPs, in order to construct a photo-enzyme integrated catalyst (denoted as $mTiO_2$ -CVs2.5@lac) and realize the combination of the advantages of the two kinds catalysts.

Because the $mTiO_2$ -CVs microspheres have large specific surface area and the pore volume matches well the laccase molecule size (about $6.5 \times 5.5 \times 4.5$ nm) [52], and then the laccase is immobilized on $mTiO_2$ -CVs2.5 by adsorption method. It is worth mentioning that the unique cracked mesoporous structure of $mTiO_2$ -CVs can not only realize multiple reflection of light to improve absorption, but also make the solution quickly permeate to promote laccase immobilization. The enzyme activity of $mTiO_2$ -CVs2.5@lac is usually affected by immobilized conditions such as initial enzyme concentration, adsorption time, temperature and pH during the immobilized process. The conditions have been optimized and the results are given in Fig. S5. On the basis of these results, the optimum conditions for laccase immobilization on $mTiO_2$ -CVs2.5 are as follows: the laccase concentration is 0.25 mg/mL, the adsorption time is 15 min, the initial pH is 4.5 and the temperature is 25°C. Several characterizations of $mTiO_2$ -CVs2.5@lac (such as EDS mapping, XPS, FT-IR and CLSM as shown in Fig. S6-9) confirm the successful immobilization and the uniform distribution of laccase on $mTiO_2$ -CVs2.5 microspheres. In addition, the XRD patterns of $mTiO_2$ -CVs2.5 and $mTiO_2$ -CVs2.5@lac indicate that the im-

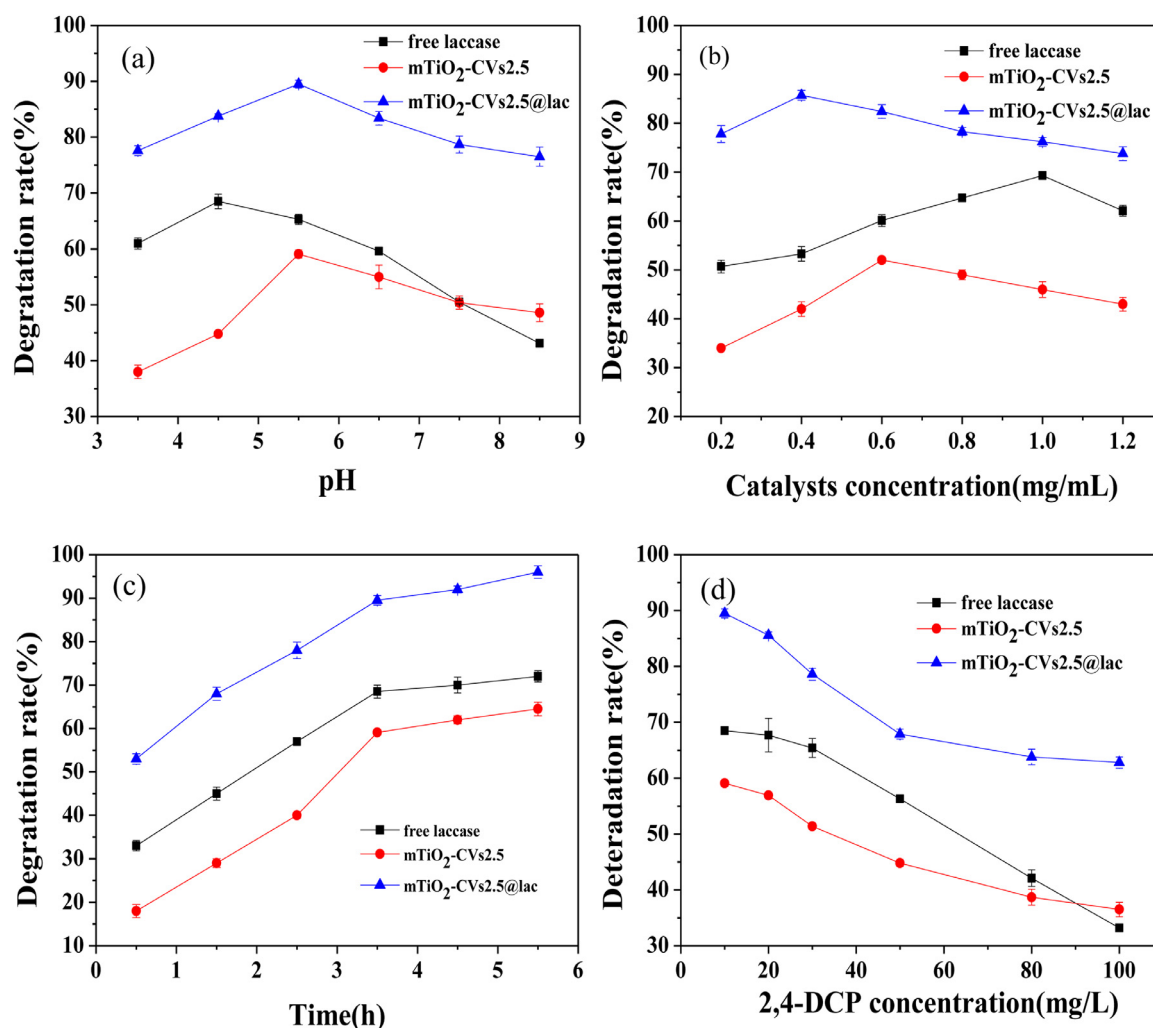


Fig. 10. Photocatalytic degradation curves of 2,4-DCP under visible light irradiation with different pH (a); Photocatalytic degradation curves of 2,4-DCP under visible light irradiation with different amount of catalysts (b); Photocatalytic degradation curves of 2,4-DCP under visible light irradiation with different degradation time (c); Photocatalytic degradation curves of 2,4-DCP under visible light irradiation with different 2,4-DCP concentrations (d).

mobilization process of laccase does not significantly change the crystal structure of mTiO₂-CVs2.5 (Fig. S10).

3.4. Degradation of 2,4-DCP by photo-enzyme integrated catalyst

After optimization of the laccase immobilization process, the obtained integrated catalyst mTiO₂-CVs2.5@lac is used in photo-enzymatic synergistic degrading 2,4-DCP under visible light. The influence of reaction conditions on degradation rate of 2,4-DCP are investigated. The 2,4-DCP degradation catalyzed by free laccase and mTiO₂-CVs2.5 are used as control experiments.

As a typical biocatalyst, the conformation of laccase molecules can be affected by pH. The wide range of pH in wastewater also has influence on catalytic efficiency. Thus, the 2,4-DCP degradation by mTiO₂-CVs2.5@lac, mTiO₂-CVs2.5 and free laccase are studied under different pH conditions from 2.5 to 8.5 (Fig. 10a). The highest degradation rates of mTiO₂-CVs2.5@lac, mTiO₂-CVs2.5 and laccase are 89.5%, 59.1% and 68.5%, respectively. The degradation rate by mTiO₂-CVs2.5@lac and mTiO₂-CVs2.5 reach the highest value both at pH 5.5, while the highest degradation rate for free laccase is reached at pH 4.5. It is worth mentioning that the mTiO₂-CVs2.5@lac shows higher degradation rate of 2,4-DCP under all selected pH conditions compared to mTiO₂-CVs2.5 and free laccase. These results indicate that the laccase immobilized on mTiO₂-

CVs2.5 not only improves the stability of laccase, but also achieves good synergistic effects in the 2,4-DCP degradation.

The 2,4-DCP degradation rate by various amounts of different catalysts within 3.5 h is presented in Fig. 10b. With the increase of catalyst amount, the corresponding 2,4-DCP degradation rate increases and gradually reaches equilibrium or even declines. The degradation rate that catalyzed by mTiO₂-CVs2.5@lac is higher than that of mTiO₂-CVs2.5 and free laccase at the same dosage. Usually, with the increase of catalyst amount, there are more active sites in the reaction system and higher probability of collision between substrate molecules and the catalyst, which is beneficial for the 2,4-DCP degradation. After reacting some time, the number of active sites greatly exceeds the reaction demand and the efficiency is no longer improved. In addition, excessive mTiO₂-CVs2.5@lac or mTiO₂-CVs2.5 leads to the turbidity of the reaction system, which may shield the incident sunlight and cause decrease in photocatalytic efficiency. The inevitable agglomeration of mTiO₂-CVs2.5@lac, mTiO₂-CVs2.5 or laccase in excess is another reason that the degradation rate is no longer increased or even decreased.

From Fig. 10c, the 2,4-DCP degradation rate by mTiO₂-CVs2.5@lac, mTiO₂-CVs2.5 and free laccase with different degradation time are investigated. At the beginning of the reaction, due to the high content of 2,4-DCP and abundant active sites supplied by catalyst in the reaction system, the degradation rate increases

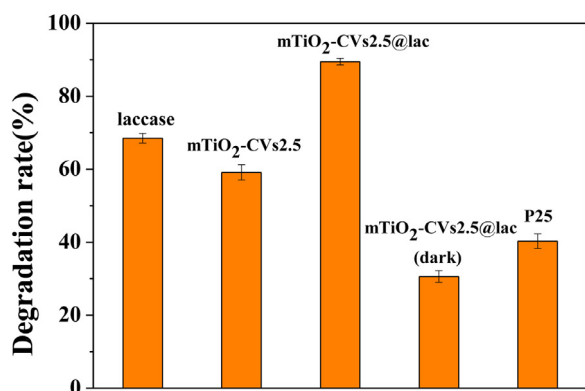


Fig. 11. Degradation of 2,4-DCP (10 mg/L; pH=5.5) with different catalysts under visible light.

rapidly. When the reaction time is 3.5 h, the 2,4-DCP degradation rate by mTiO₂-CVs2.5@lac, mTiO₂-CVs2.5 and free laccase reaches 89.5%, 59.1% and 68.5%, respectively. With the progress of reaction, the 2,4-DCP degradation rate increases more and more slowly, and the maximum degradation rate of 2,4-DCP by mTiO₂-CVs2.5@lac, mTiO₂-CVs2.5 and free laccase reaches 96.8%, 64.5% and 72.3%, respectively. These results further indicate that the degradation rate by the integrated catalyst mTiO₂-CVs2.5@lac is remarkably higher and faster than the process catalyzed by mTiO₂-CVs2.5 or free laccase used separately.

Fig. 10d indicates the 2,4-DCP degradation with various initial concentration ranging from 10 to 100 mg/L catalyzed by mTiO₂-CVs2.5@lac, mTiO₂-CVs2.5 and free laccase. As the initial concentration increases, the substrate inhibition is gradually increased. Compared to mTiO₂-CVs2.5 and free laccase, mTiO₂-CVs2.5@lac reacts rapidly and almost completely degrades 2,4-DCP at low concentration, and maintains an efficient degradation effect at high concentration. These results can be ascribed to the integration of photocatalysis and enzyme catalysis in mTiO₂-CVs2.5@lac, which endows that mTiO₂-CVs2.5@lac possess better catalytic property than mTiO₂-CVs2.5 and free laccase.

The 2,4-DCP degradation catalyzed by various catalytic methods including photo-enzymatic catalysis (mTiO₂-CVs2.5@lac under light irradiation), photocatalysis (mTiO₂-CVs2.5 under light irradiation) and enzymatic catalysis (mTiO₂-CVs2.5@lac under dark condition) are further studied and compared. Commercial P25 and free laccase are used in control experiments. As shown in Fig. 11, the photo-enzymatic catalysis by mTiO₂-CVs2.5@lac under visible light irradiation shows the best degradation rate of 89.5% within 3.5 h, which is much higher than that of the commercial P25 (46.8%), mTiO₂-CVs2.5 (59.1%), free laccase (68.5%) and mTiO₂-CVs2.5@lac (30.6%, under dark condition). The improved degradation performance of mTiO₂-CVs2.5@lac are mainly ascribed to the following reasons: (1) The effective utilization of visible light and unique cluster porous structure of mTiO₂-CVs2.5 can effectively avoid the damage of ultraviolet radiation to laccase in the photocatalytic process, which has been recognized as the main obstacle to the synergistic reaction between enzyme and TiO₂ in previous studies. (2) The construction of the integrated catalyst realizes the effective coordination of photocatalysis and enzyme catalysis, the degradation process occurs simultaneously and promotes each other. (3) The immobilization of laccase molecules in the pores of mTiO₂-CVs2.5 makes the photocatalytic active site and the enzymatic active site appear in the same space, and this proximity effect can accelerate the transport of charge carriers and also the intermediate products in the two catalytic reactions, thus improving the degradation rate. (4) The porous structure of mTiO₂-CVs2.5 can well protect the advanced structure of laccase molecules from being destroyed by

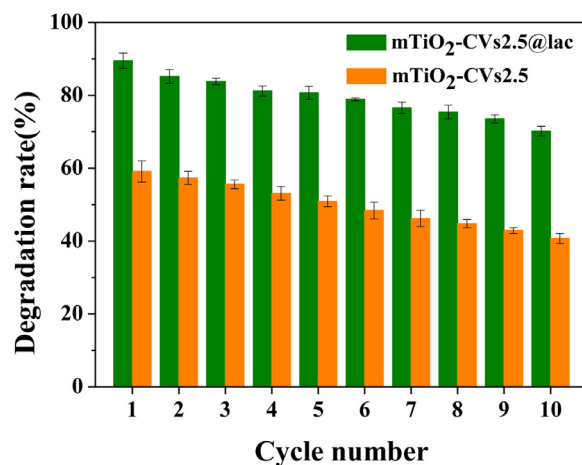


Fig. 12. The reusability of mTiO₂-CVs2.5@lac and mTiO₂-CVs2.5.

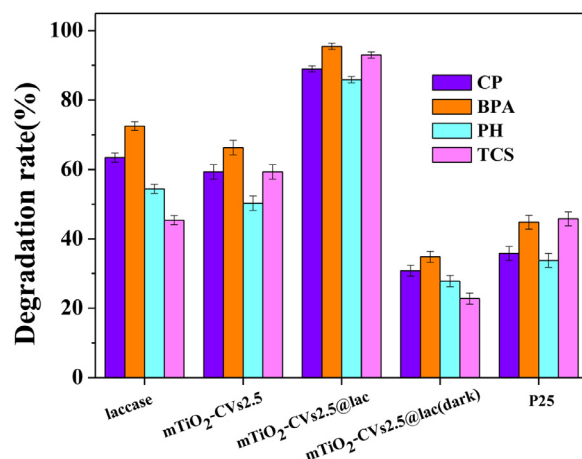


Fig. 13. Degradation rate of mTiO₂-CVs2.5@lac towards CP, BPA, PH and TCS.

UV irradiation. In addition, the distribution of enzyme molecules in porous structures can effectively prevent the leakage of enzyme molecules in the catalytic process.

3.5. The reusability of mTiO₂-CVs2.5@lac and mTiO₂-CVs2.5

Fig. 12 shows the 2,4-DCP degradation rate catalyzed by mTiO₂-CVs2.5 and mTiO₂-CVs2.5@lac (3.5 h each) under visible light illumination. The 2,4-DCP degradation rates catalyzed by mTiO₂-CVs2.5@lac and mTiO₂-CVs2.5 retain 71.2% and 40.6% after 10 cycles of reactions, respectively. Furthermore, the crystal phases, element compositions and valence states are used to analyze the properties of the recovered mTiO₂-CVs2.5@lac and mTiO₂-CVs2.5 after the reactions. These results show that the performance and characteristics of the mTiO₂-CVs2.5@lac and mTiO₂-CVs2.5 remain relatively unchanged during the long-term reaction and irradiation, and thus possess outstanding stability for the degradation of 2,4-DCP.

3.6. Preliminary discussions on the mechanism

Based on the above-mentioned experimental results, mTiO₂-CVs@lac possess favorable catalytic activity in 2,4-DCP degradation. The possible mechanism of synergistic degradation is shown in Scheme 1. It is well known that there are numerous main ROS when heterophase mTiO₂-CVs2.5@lac are excited by visible light, such as h⁺, •OH and •O₂⁻. The active species trapping experiments

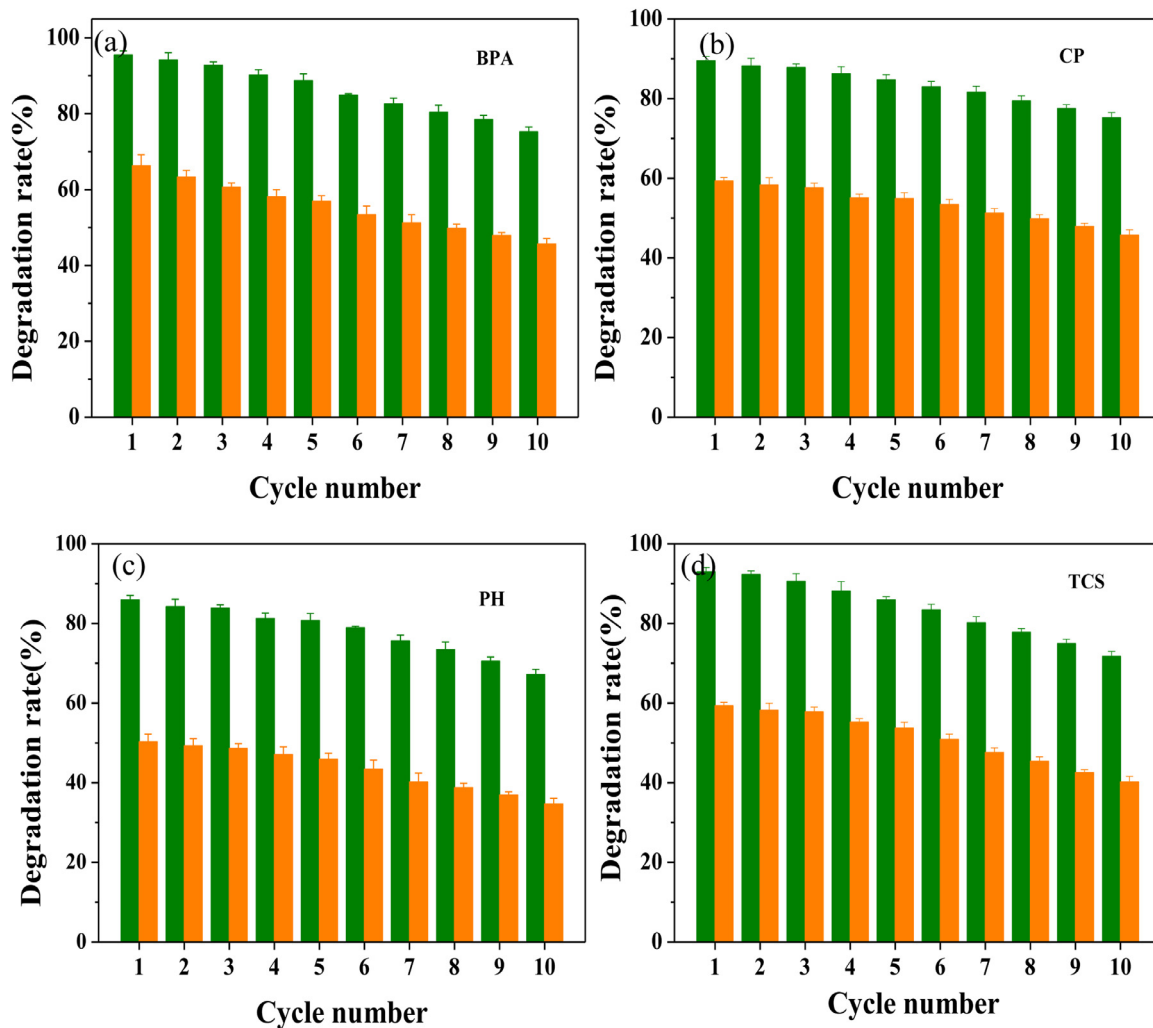
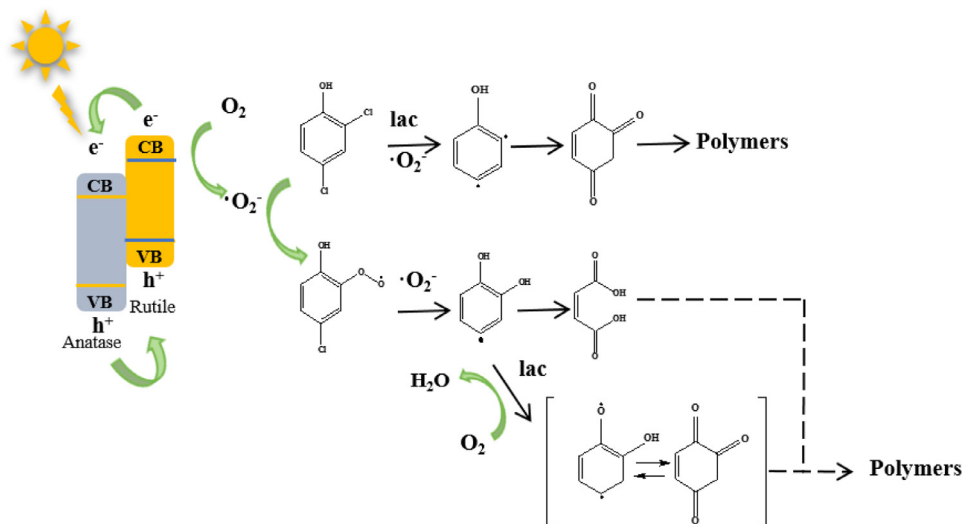


Fig. 14. The reusability of mTiO₂-CVs2.5@lac and mTiO₂-CVs2.5 on (a) BPA, (b) CP, (c) PH and (d) TCS.



Scheme 1. Possible degradation mechanism of 2,4-DCP catalyzed by mTiO₂-CVs2.5@lac under visible light irradiation.

confirm that the $\bullet\text{O}_2^-$ is the main ROS in the photocatalytic reaction. The superoxide radical generated by $\text{mTiO}_2\text{-CVs}$ under light radiation can reduce and decompose the chlorinated phenol polymer in the polymerization. 2,4-DCP is gradually dechlorinated to form p-chlorophenol superoxide radical and 2-hydroxyphenol and further generate cyclohexanol and cyclohexanone due to the attack of ortho or para-chloride by the $\bullet\text{O}_2^-$ generated from $\text{mTiO}_2\text{-CVs}$, and finally decompose into low alcohols, acids and ketones. As reported in the literature, the toxicity of intermediate substances such as p-chlorophenol superoxide radical and 2-hydroxyphenol is less than that of 2, 4-DCP [5]. Meanwhile, laccase can catalyze the oxidation of phenolics compounds by generating phenoxy radicals, and eventually convert the substrate to higher oligomers and polymers of low solubility, which easily removed by sedimentation or filtration [53]. During the 2,4-DCP degradation process catalyzed by laccase, Cu ions at the active site of T1 absorb electrons from 2,4-DCP and oxidize the substrate to form phenoxy radicals, leading to the non-enzymatic secondary polymerization [54-56]. Laccase can catalyze the intermediate compounds from photocatalysis to form separable polymer [55]. Thus, the overall degradation reaction of 2,4-DCP is accelerated through the combination of the two catalytic processes, showing better degradation rate than any single catalyst. In addition, the obtained $\text{mTiO}_2\text{-CVs}$ have a heterophase crystal structure and unique cluster porous structure, which can effectively utilize visible light and protect the enzyme molecules so that the overall reaction can be carried out simultaneously.

3.7. Universal applicability

Meanwhile, in order to demonstrate that the designed $\text{mTiO}_2\text{-CVs2.5@lac}$ have extensive degradation ability, 4-chlorophenol (CP), bisphenol A (BPA), phenol (PH) and triclosan (TCS) are chose as model EOCs for degradation test. Fig. 13 shows the degradation results of the four pollutants. The $\text{mTiO}_2\text{-CVs2.5@lac}$ displays a favorable degradation property towards CP, BPA, PH and TCS. The degradation rate of CP, BPA, PH and TCS catalyzed by $\text{mTiO}_2\text{-CVs2.5@lac}$ is 89.0%, 95.5%, 85.9% and 93.0%, respectively, after 3.5 h of reaction. The results prove that the $\text{mTiO}_2\text{-CVs2.5@lac}$ can be used for the degradation of various EOCs in water.

The reusability experiments of $\text{mTiO}_2\text{-CVs2.5@lac}$ and $\text{mTiO}_2\text{-CVs2.5}$ for degrading CP, BPA, PH and TCS were also conducted. It can be seen from Fig. 14 that the catalytic activities of $\text{mTiO}_2\text{-CVs2.5@lac}$ and $\text{mTiO}_2\text{-CVs2.5}$ do not decrease significantly after 10 cycles of reactions. These results further prove that $\text{mTiO}_2\text{-CVs2.5@lac}$ and $\text{mTiO}_2\text{-CVs2.5}$ not only has universal applicability but also has outstanding reusability.

4. Conclusions

In conclusion, a novel controllable heterophase porous TiO_2 microsphere with ordered regular radial structure is prepared. The obtained $\text{mTiO}_2\text{-CVs2.5}$ is used to construct photo-enzyme integrated catalyst by immobilizing laccase in the pores of $\text{mTiO}_2\text{-CVs2.5}$ for the first time. Compared with the commercial P25 and ordinary TiO_2 , the $\text{mTiO}_2\text{-CVs}$ has a narrower band gap, and can realize the effective utilization of visible light and exhibit better photocatalytic activity. Moreover, the $\text{mTiO}_2\text{-CVs}$ have regular morphology, large specific surface area, good biocompatibility which can match and protect laccase molecules well. The integrated catalyst ($\text{mTiO}_2\text{-CVs2.5@lac}$) is applied in the effective degradation of 2,4-DCP, CP, BPA, PH and TCS under visible light and shows a higher catalytic efficiency than the single catalytic method. By using the novel integrated catalyst under visible light, not only the coordination and promotion of the two catalytic methods are realized, but also the loss of enzyme activity caused by ultraviolet

light can be reduced. These results indicate that the two green and energy-saving catalytic technologies can be effectively combined through this method. This photo-enzyme integrated catalyst can be widely used to the emerging organic contaminants in water. This research also provides a simple, effective and constructive path for the integration of different catalytic methods.

Notes

The authors declare no competing financial interest.

Credit author statement

Ying Zhang: Experimental design and planning, performing the experiments, data visualization, writing the initial draft and revised manuscript. **Jing Gao:** Formulation of overarching research goals and aims, validating result and data collation. **Xin Xin:** Performing the experiments. **Lihui Wang:** Analyzing study data. **Heyu Li:** Provision of study materials, reagents, materials. **Xiaobing Zheng:** Ideas, revised the initial draft and revised the initial draft. **Yanjun Jiang:** Ideas, oversight and leadership responsibility for the research activity planning and execution, revised the initial draft and funding acquisition

Declaration of Competing Interest

The authors declare that they have no known competing financial interests or personal relationships that could have appeared to influence the work reported in this paper.

Acknowledgments

This work was supported by the National Natural Science Foundation of China [No. 21576068 and 21878068]; the Natural Science Foundation of Hebei Province [B2015202082 and B2017202056]; the Program for Top 100 Innovative Talents in Colleges and Universities of Hebei Province [SLRC2017029] and Hebei High Level Personnel of Support Program [A2016002027]; National College Student's Science and Technology Innovation Project [201910080027].

Supplementary materials

Supplementary material associated with this article can be found, in the online version, at doi:10.1016/j.apmt.2020.100810.

References

- [1] X.Y. Shu, Q. Yang, F.B. Yao, Y. Zhong, W.C. Ren, F. Chen, J. Sue, Y.H. Ma, Z.Y. Fe, D.B. Wang, X.M. Li, Electrocatalytic hydrodechlorination of 4-chlorophenol on Pd supported multi-walled carbon nanotubes particle electrodes, Chem. Eng. J. 358 (2019) 903-911, doi:10.1016/j.cej.2018.10.095.
- [2] M. Humayun, Z. Hu, A. Khan, W. Cheng, Y. Yuan, Z. Zheng, Q. Fu, W. Luo, Highly efficient degradation of 2,4-dichlorophenol over $\text{CeO}_2/\text{g-C}_3\text{N}_4$ composites under visible-light irradiation: Detailed reaction pathway and mechanism, J. Hazard. Mater. 364 (2019) 635-644, doi:10.1016/j.jhazmat.2018.10.088.
- [3] K.J. Li, Y. Yang, A.U.R. Bacha, Y.Q. Feng, S. Ajmal, I. Nabi, L.W. Zhang, Efficiently complete degradation of 2,4-DCP using sustainable photoelectrochemical reduction and sequential oxidation method, Chem. Eng. J. 378 (2019) 122191, doi:10.1016/j.cej.2019.122191.
- [4] X. Li, M. Zhou, Y. Pan, L.J.C.E.J. Xu, Pre-magnetized Fe^0 /persulfate for notably enhanced degradation and dechlorination of 2,4-dichlorophenol, Chem. Eng. J. 307 (2017) 1092-1104, doi:10.1016/j.cej.2016.08.140.
- [5] M.N. Chu, K. Hu, J.S. Wang, Y.D. Liu, S. Ali, C.L. Qin, L.Q. Jing, Synthesis of g- C_3N_4 -based photocatalysts with recyclable feature for efficient 2,4-dichlorophenol degradation and mechanisms, Appl. Catal. B-Environ. 243 (2019) 57-65, doi:10.1016/j.apcatb.2018.10.008.
- [6] C.A. Martinez-Huitle, E. Brillas, Decontamination of wastewaters containing synthetic organic dyes by electrochemical methods: A general review, Appl. Catal. B-Environ. 87 (2009) 105-145, doi:10.1016/j.apcatb.2008.09.017.

- [7] X. Yu, D. Cabooter, R. Dewil, Effects of process variables and kinetics on the degradation of 2,4-dichlorophenol using advanced reduction processes (ARP), *J. Hazard. Mater.* 357 (2018) 81–88, doi:[10.1016/j.jhazmat.2018.05.049](https://doi.org/10.1016/j.jhazmat.2018.05.049).
- [8] Y. Liu, Z. Yan, R. Chen, Y. Yu, X. Chen, X. Zheng, X. Huang, 2,4-Dichlorophenol removal from water using an electrochemical method improved by a composite molecularly imprinted membrane/bipolar membrane, *J. Hazard. Mater.* 377 (2019) 259–266, doi:[10.1016/j.jhazmat.2019.05.064](https://doi.org/10.1016/j.jhazmat.2019.05.064).
- [9] J.H. Wang, R.L. Huang, W. Qi, R.X. Su, B.P. Binks, Z.M. He, Construction of a bioinspired laccase-mimicking nanozyme for the degradation and detection of phenolic pollutants, *Appl. Catal. B-Environ.* 254 (2019) 452–462, doi:[10.1016/j.apcatb.2019.05.012](https://doi.org/10.1016/j.apcatb.2019.05.012).
- [10] S. Karthikeyan, C.J. Magthalin, A.B. Mandal, G. Sekaran, Controlled synthesis and characterization of electron rich iron(III) oxide doped nanoporous activated carbon for the catalytic oxidation of aqueous ortho phenylene diamine, *RSC Adv.* 4 (2014) 19183–19195, doi:[10.1039/C4RA00754A](https://doi.org/10.1039/C4RA00754A).
- [11] Y. Wu, H. Wang, W.G. Tu, Y. Liu, S.Y. Wu, Y.Z. Tan, J.W. Chew, Construction of hierarchical 2D-2D Zn₃In₂S₆/fluorinated polymeric carbon nitride nanosheets photocatalyst for boosting photocatalytic degradation and hydrogen production performance, *Appl. Catal. B-Environ.* 233 (2018) 58–69, doi:[10.1016/j.apcatb.2018.03.105](https://doi.org/10.1016/j.apcatb.2018.03.105).
- [12] L. Sun, T. Du, C. Hu, J. Chen, J. Lu, Z. Lu, H. Han, Antibacterial activity of graphene oxide/g-C₃N₄ composite through photocatalytic disinfection under visible light, *ACS Sustain. Chem. Eng.* 5 (2017) 8693–8701, doi:[10.1021/acsschemeng.7b01431](https://doi.org/10.1021/acsschemeng.7b01431).
- [13] A. Chenchana, A. Nemancha, H. Moumeni, J.M. Doña Rodríguez, J. Araña, J.A. Navío, O. González Díaz, E. Pulido Melián, Photodegradation of 2,4-dichlorophenoxyacetic acid over TiO₂(B)/anatase nanobelts and Au-TiO₂(B)/anatase nanobelts, *Appl. Surf. Sci.* 467–468 (2019) 1076–1087, doi:[10.1016/j.apsusc.2018.10.175](https://doi.org/10.1016/j.apsusc.2018.10.175).
- [14] B. Sun, W. Zhou, H. Li, L. Ren, P. Qiao, W. Li, H. Fu, Synthesis of particulate hierarchical tandem heterojunctions toward optimized photocatalytic hydrogen production, *Adv. Mater.* 30 (2018) 1804282, doi:[10.1002/adma.201804282](https://doi.org/10.1002/adma.201804282).
- [15] J.J. Yu, T.H. Wang, S. Rtimi, Magnetically separable TiO₂/FeOx/POM accelerating the photocatalytic removal of the emerging endocrine disruptor: 2,4-dichlorophenol, *Appl. Catal. B-Environ.* 254 (2019) 66–75, doi:[10.1016/j.apcatb.2019.04.088](https://doi.org/10.1016/j.apcatb.2019.04.088).
- [16] M.J. Chen, S.L. Lo, Y.C. Lee, C.C. Huang, Photocatalytic decomposition of perfluorooctanoic acid by transition-metal modified titanium dioxide, *J. Hazard. Mater.* 288 (2015) 168–175, doi:[10.1016/j.jhazmat.2015.02.004](https://doi.org/10.1016/j.jhazmat.2015.02.004).
- [17] R. Asahi, T. Morikawa, T.J.S. Ohwaki, Visible-light photocatalysis in nitrogen-doped titanium oxides, *Appl. Surf. Sci.* 293 (2020) 269–271, doi:[10.1126/science.1061051](https://doi.org/10.1126/science.1061051).
- [18] H. Liu, W. Li, D. Shen, D. Zhao, G. Wang, Graphitic carbon conformal coating of mesoporous TiO₂ hollow spheres for high-performance lithium ion battery anodes, *J. Am. Chem. Soc.* 137 (2015) 13161–13166, doi:[10.1021/jacs.5b08743](https://doi.org/10.1021/jacs.5b08743).
- [19] X.D. Jiang, Y.P. Zhang, J. Jiang, Y.S. Rong, Y.C. Wang, Y.C. Wu, C.X. Pan, Characterization of oxygen vacancy associates within hydrogenated TiO₂: A positron annihilation study, *J. Phys. Chem. C* 116 (2012) 22619–22624, doi:[10.1021/jp307573c](https://doi.org/10.1021/jp307573c).
- [20] S. Bai, N. Zhang, C. Gao, Y.J. Xiong, Defect engineering in photocatalytic materials, *Nano Energy* 53 (2018) 296–336, doi:[10.1016/j.nanoen.2018.08.058](https://doi.org/10.1016/j.nanoen.2018.08.058).
- [21] L. Ren, W. Zhou, B. Sun, H. Li, P. Qiao, Y. Xu, J. Wu, K. Lin, H. Fu, Defects-engineering of magnetic γ -Fe₂O₃ ultrathin nanosheets/mesoporous black TiO₂ hollow sphere heterojunctions for efficient charge separation and the solar-driven photocatalytic mechanism of tetracycline degradation, *Appl. Catal. B-Environ.* 240 (2019) 319–328, doi:[10.1016/j.apcatb.2018.08.033](https://doi.org/10.1016/j.apcatb.2018.08.033).
- [22] Y. Cho, S. Kim, B. Park, C.L. Lee, J.K. Kim, K.S. Lee, I.Y. Choi, J.K. Kim, K. Zhang, S.H. Oh, J.H. Park, Multiple heterojunction in single titanium dioxide nanoparticles for novel metal-free photocatalysis, *Nano Lett.* 18 (2018) 4257–4262, doi:[10.1021/acs.nanolett.8b01245](https://doi.org/10.1021/acs.nanolett.8b01245).
- [23] J. Dai, J. Yang, X.H. Wang, L. Zhang, Y.J. Li, Enhanced visible-light photocatalytic activity for selective oxidation of amines into imines over TiO₂(B)/anatase mixed-phase nanowires, *Appl. Surf. Sci.* 349 (2015) 343–352, doi:[10.1016/j.apsusc.2015.04.232](https://doi.org/10.1016/j.apsusc.2015.04.232).
- [24] R. Hao, B.J. Jiang, M.X. Li, Y. Xie, H.G. Fu, Fabrication of mixed-crystalline-phase spindle-like TiO₂ for enhanced photocatalytic hydrogen production, *Sci. China-Mater.* 58 (2015) 363–369, doi:[10.1007/s40843-015-0052-3](https://doi.org/10.1007/s40843-015-0052-3).
- [25] K. Li, J.H. Wang, Y.J. He, G.L. Cui, M.A. Abdulrazaq, Y.J. Yan, Enhancing enzyme activity and enantioselectivity of Burkholderia cepacia lipase via immobilization on melamine-glutaraldehyde dendrimer modified magnetic nanoparticles, *Chem. Eng. J.* 351 (2018) 258–268, doi:[10.1016/j.cej.2018.06.086](https://doi.org/10.1016/j.cej.2018.06.086).
- [26] D. Alba-Molina, D. Rodríguez-Padron, A.R. Puentes-Santiago, J.J. Giner-Casares, M.T. Martín-Romero, L. Camacho, L.O. Martins, M.J. Muñoz-Batista, M. Cano, R. Luque, Mimicking the bioelectrocatalytic function of recombinant CotA laccase through electrostatically self-assembled bioconjugates, *Nanoscale* 11 (2019) 1549–1554, doi:[10.1039/C8NR06001K](https://doi.org/10.1039/C8NR06001K).
- [27] G.H. Li, A.G. Nandgaonkar, Q.Q. Wang, J.N. Zhang, W.E. Krause, Q.F. Wei, L.A. Lucia, Laccase-immobilized bacterial cellulose/TiO₂ functionalized composite membranes: Evaluation for photo- and bio-catalytic dye degradation, *J. Membrane Sci.* 525 (2017) 89–98, doi:[10.1016/j.memsci.2016.10.033](https://doi.org/10.1016/j.memsci.2016.10.033).
- [28] N. Durán, M.A. Rosa, A. D'Annibale, L.J.E. Gianfreda, M. Technology, Applications of laccases and tyrosinases (phenoloxidases) immobilized on different supports: a review, *Enzyme Microb. Tech.* 31 (2002) 907–931, doi:[10.1016/S0141-0229\(02\)00214-4](https://doi.org/10.1016/S0141-0229(02)00214-4).
- [29] D.S. Jiang, S.Y. Long, J. Huang, H.Y. Xiao, J.Y. Zhou, Immobilization of pycnopus sanguineus laccase on magnetic chitosan microspheres, *Biochem. Eng. J.* 25 (2005) 15–23, doi:[10.1016/j.bej.2005.03.007](https://doi.org/10.1016/j.bej.2005.03.007).
- [30] F. Wang, C. Guo, L.R. Yang, C.Z. Liu, Magnetic mesoporous silica nanoparticles: Fabrication and their laccase immobilization performance, *Bioresource Technol.* 101 (2010) 8931–8935, doi:[10.1016/j.biortech.2010.06.115](https://doi.org/10.1016/j.biortech.2010.06.115).
- [31] H.J. Qiu, C.X. Xu, X.R. Huang, Y. Ding, Y.B. Qu, P.J. Gao, Adsorption of laccase on the surface of nanoporous gold and the direct electron transfer between them, *J. Phys. Chem. C* 112 (2008) 14781–14785, doi:[10.1021/jp805600k](https://doi.org/10.1021/jp805600k).
- [32] Y. Chen, P. Li, J. Zhou, C.T. Buru, L. Dordevic, P. Li, X. Zhang, M.M. Cetin, J.F. Stoddart, S.I. Stupp, M.R. Wasielewski, O.K. Farha, Integration of enzymes and photosensitizers in a hierarchical mesoporous metal-organic framework for light-driven CO₂ reduction, *J. Am. Chem. Soc.* 142 (2020) 1768–1773, doi:[10.1021/jacs.9b12828](https://doi.org/10.1021/jacs.9b12828).
- [33] Z.C. Litman, Y. Wang, H. Zhao, J.F. Hartwig, Cooperative asymmetric reactions combining photocatalysis and enzymatic catalysis, *Nature* 560 (2018) 355–359, doi:[10.1038/s41586-018-0413-7](https://doi.org/10.1038/s41586-018-0413-7).
- [34] L. Schermund, V. Jurkas, F.F. Ozgen, G.D. Barone, H.C. Buchsenschutz, C.K. Winkler, S. Schmidt, R. Kourist, W. Kroutil, Photo-Biocatalysis: Biotransformations in the presence of light, *ACS Catal.* 9 (2019) 4115–4144, doi:[10.1038/s41586-018-0413-7](https://doi.org/10.1038/s41586-018-0413-7).
- [35] J.F. Allen, W.B. de Paula, S. Puthiyaveetil, J. Nield, A structural phylogenetic map for chloroplast photosynthesis, *Trends Plant Sci.* 16 (2011) 645–655, doi:[10.1016/j.tplants.2011.10.004](https://doi.org/10.1016/j.tplants.2011.10.004).
- [36] K. Lan, R.C. Wang, W. Zhang, Z.W. Zhao, A. Elzatahy, X.M. Zhang, Y. Liu, D. Al-Dhayyan, Y.Y. Xia, D.Y. Zhao, Mesoporous TiO₂ microspheres with precisely controlled crystallites and architectures, *Chem-Us* 4 (2018) 2436–2450, doi:[10.1016/j.chempr.2018.08.008](https://doi.org/10.1016/j.chempr.2018.08.008).
- [37] W. Zhang, H. He, Y. Tian, K. Lan, Q. Liu, C. Wang, Y. Liu, A. Elzatahy, R. Che, W. Li, D. Zhao, Synthesis of uniform ordered mesoporous TiO₂ microspheres with controllable phase junctions for efficient solar water splitting, *Chem. Sci.* 10 (2019) 1664–1670, doi:[10.1039/C8SC04155E](https://doi.org/10.1039/C8SC04155E).
- [38] W. Zhou, W. Li, J.-Q. Wang, Y. Qu, Y. Yang, Y. Xie, K. Zhang, L. Wang, H. Fu, D. Zhao, Ordered mesoporous black TiO₂ as highly efficient hydrogen evolution photocatalyst, *J. Am. Chem. Soc.* 136 (2014) 9280–9283, doi:[10.1021/ja504802q](https://doi.org/10.1021/ja504802q).
- [39] W. Zhang, H.L. He, Y. Tian, H.Z. Li, K. Lan, L.H. Zu, Y. Xia, L.L. Duan, W. Li, D.Y. Zhao, Defect-engineering of mesoporous TiO₂ microspheres with phase junctions for efficient visible-light driven fuel production, *Nano Energy* 66 (2019) 104113, doi:[10.1016/j.nanoen.2019.104113](https://doi.org/10.1016/j.nanoen.2019.104113).
- [40] Y.L. Bai, R. Xarapatgl, X.Y. Wu, X. Liu, Y.S. Liu, K.X. Wang, J.S. Chen, Core-shell anatase anode materials for sodium-ion batteries: the impact of oxygen vacancies and nitrogen-doped carbon coating, *Nanoscale* 11 (2019) 17860–17868, doi:[10.1039/C9NR06245A](https://doi.org/10.1039/C9NR06245A).
- [41] Q.F. Chen, H. Wang, C.C. Wang, R.F. Guan, R. Duan, Y.F. Fang, X. Hu, Activation of molecular oxygen in selectively photocatalytic organic conversion upon defective TiO₂ nanosheets with boosted separation of charge carriers, *Appl. Catal. B-Environ.* 262 (2020) 118258, doi:[10.1016/j.apcatb.2019.118258](https://doi.org/10.1016/j.apcatb.2019.118258).
- [42] H. Che, L. Liu, G. Che, H. Dong, C. Liu, C. Li, Control of energy band, layer structure and vacancy defect of graphitic carbon nitride by intercalated hydrogen bond effect of NO₃⁻ toward improving photocatalytic performance, *Chem. Eng. J.* 357 (2019) 209–219, doi:[10.1016/j.cej.2018.09.112](https://doi.org/10.1016/j.cej.2018.09.112).
- [43] X.R. Jiang, Z.Y. Yan, J. Zhang, J.Z. Gao, W.X. Huang, Q.W. Shi, H.Z. Zhang, Mesoporous hollow black TiO₂ with controlled lattice disorder degrees for highly efficient visible-light-driven photocatalysis, *RSC Adv.* 9 (2019) 36907–36914, doi:[10.1039/C9RA08148H](https://doi.org/10.1039/C9RA08148H).
- [44] J. Lyu, L. Zhou, J.W. Shao, Z. Zhou, J.X. Gao, Y.M. Dong, Z.Y. Wang, J. Li, TiO₂ hollow heterophase junction with enhanced pollutant adsorption, light harvesting, and charge separation for photocatalytic degradation of volatile organic compounds, *Chem. Eng. J.* (2019) 123602, doi:[10.1016/j.cej.2019.123602](https://doi.org/10.1016/j.cej.2019.123602).
- [45] M. Kruk, M. Jaroniec, Gas adsorption characterization of ordered organic-inorganic nanocomposite materials, *Chem. Mater.* 13 (2001) 3169–3183, doi:[10.1021/cm0101069](https://doi.org/10.1021/cm0101069).
- [46] H.M. Cheng, J.M. Ma, Z.G. Zhao, L.M. Qi, Hydrothermal preparation of uniform nanosize rutile and anatase particles, *Chem. Mater.* 7 (1995) 663–671, doi:[10.1021/cm00052a010](https://doi.org/10.1021/cm00052a010).
- [47] S.S. Shaik, P.C. Hiberty, J.M. Lefour, G.J.C. Ohanessian, Cheminform abstract: Is delocalization a driving force in chemistry? benzene, allyl radical, cyclobutadiene, and their isoelectronic species, *J. Am. Chem. Soc.* 109 (1987) 363–374, doi:[10.1002/chin.198722053](https://doi.org/10.1002/chin.198722053).
- [48] T.S. Rajaraman, S.P. Parikh, V.G. Gandhi, Black TiO₂, A review of its properties and conflicting trends, *Chem. Eng. J.* 389 (2020) 123918, doi:[10.1016/j.cej.2019.123918](https://doi.org/10.1016/j.cej.2019.123918).
- [49] J. Zhang, X.B. Chen, Y. Bai, C. Li, Y. Gao, R.G. Li, C. Li, Boosting photocatalytic water splitting by tuning built-in electric field at phase junction, *J. Mater. Chem. A* 7 (2019) 10264–10272, doi:[10.1039/C8TA08199A](https://doi.org/10.1039/C8TA08199A).
- [50] D.C. Hurum, A.G. Agrios, K.A. Gray, T. Rajh, M.C. Thurnauer, Explaining the enhanced photocatalytic activity of degussa P25 mixed-phase TiO₂ using EPR, *J. Phys. Chem. B* 107 (2003) 4545–4549, doi:[10.1021/jp0273934](https://doi.org/10.1021/jp0273934).
- [51] E. Assayehegn, A. Solaiappan, Y. Chebude, E. Alemayehu, Fabrication of tunable anatase/rutile heterojunction N/TiO₂ nanophotocatalyst for enhanced visible light degradation activity, *Appl. Surf. Sci.* 515 (2020) 145966, doi:[10.1016/j.apsusc.2020.145966](https://doi.org/10.1016/j.apsusc.2020.145966).
- [52] B. Shao, Z. Liu, G. Zeng, Y. Liu, X. Yang, C. Zhou, M. Chen, Y. Jjiang, M. Yan, Immobilization of laccase on hollow mesoporous carbon nanospheres: Noteworthy immobilization, excellent stability and efficacious for antibiotic

- contaminants removal, *J. Hazard. Mater.* 362 (2019) 318–326, doi:[10.1016/j.jhazmat.2018.08.069](https://doi.org/10.1016/j.jhazmat.2018.08.069).
- [53] S.R. Couto, J.L.T. Herrera, Industrial and biotechnological applications of laccases: a review, *Biotechnol. Adv.* 24 (2006) 500–513, doi:[10.1016/j.biotechadv.2006.04.003](https://doi.org/10.1016/j.biotechadv.2006.04.003).
- [54] S.M. Jones, E.I. Solomon, Electron transfer and reaction mechanism of laccases, *Cell Mol. Life Sci.* 72 (2015) 869–883, doi:[10.1007/s00018-014-1826-6](https://doi.org/10.1007/s00018-014-1826-6).
- [55] J. Jia, S. Zhang, P. Wang, H. Wang, Degradation of high concentration 2,4-dichlorophenol by simultaneous photocatalytic-enzymatic process using TiO₂/UV and laccase, *J. Hazard. Mater.* 205–206 (2012) 150–155, doi:[10.1016/j.jhazmat.2011.12.052](https://doi.org/10.1016/j.jhazmat.2011.12.052).
- [56] R.G. Hadt, S.I. Gorelsky, E.I. Solomon, Anisotropic covalency contributions to superexchange pathways in type one copper active sites, *J. Am. Chem. Soc.* 136 (2014) 15034–15045, doi:[10.1021/ja508361h](https://doi.org/10.1021/ja508361h).